Strain relaxation at the 3*C*-SiC/Si interface: Raman scattering experiments

L. A. Falkovsky
Groupe d'Etudes des Semiconducteurs, cc074, UM2-CNRS, 34095 Montpellier cedex5, France
and Landau Institute for Theoretical Physics, Russian Academy of Sciences, Kosygina 2, Moscow 117 334, Russia

J. M. Bluet* and J. Camassel
Groupe d'Etudes des Semiconducteurs, cc074, UM2-CNRS, 34095 Montpellier cedex5, France
(Received 23 May 1997; revised manuscript received 10 September 1997)

Using micro-Raman spectroscopy we have investigated both the residual strain and strain relaxation effect in the heteroepitaxial 3*C*-SiC/Si system. To get quantitative results, we have developed a theory of inhomogeneous shift and broadening for optical phonons, which takes into account the phonon interaction with the static strain fluctuations. We solved Dyson's equation for the averaged phonon Green's function and studied the solution for a small momentum transfer near the top of the phonon branches. The Raman scattering cross section is then calculated, including both disorder and the spatial dependence of the average strain with distance from the interface. It is shown that two regimes of short- and long-range disorder, with different line shapes, can be observed. In the case of the short-range disorder, a phonon can change its momentum (in the scattering process due to strain fluctuations) in a range which is larger than the value determined by the phonon width. The opposite case corresponds to the long-range disorder. We have also considered the case of an anisotropic (two-dimensional-like) disorder which can be viewed as a set of columns perpendicular to the heterointerface. The results of our investigations show that all three regimes should have macroscopic scales. Comparing in great detail the experimental results with the theory, we have obtained a very good agreement in both cases of the singlet (LO) and doublet (TO) modes, including the cases where the lattice mismatch-induced splitting is observed. Finally we have found, from the change in coupling constant plotted versus distance from the interface, that the mean-squared strain relaxes in the bulk of our epitaxial samples according to an approximate z^{-1} dependence. [S0163-1829(98)04318-5]

I. INTRODUCTION

There is in the modern automotive, avionics, and process-control industries more and more interest in probing the environment at high temperature and under extremely rough conditions. With this respect, SiC sensors would be very much welcome. However, it will be a long way to go before 6H or 4H polytyps, grown on 6H or 4H substrates, can enter this very lucrative market.[1] This is not the case for 3*C*-SiC or Si. Despite a very large (about 20%) nominal lattice mismatch, it is now well established that cubic (3*C*) silicon carbide can be grown on large (4–6 in.) silicon wafers using heteroepitaxial chemical vapor deposition (CVD) techniques.[2] By creating a regular misfit dislocation pattern, most of the lattice mismatch is accommodated near the SiC/Si interface and only a few percent of the nominal strain remains in the two different materials. This is still a problem for mass-market applications. Indeed, in many cases, this (small) amount of residual strain induces a large bending of the initial wafer which precludes any further processing step. This makes useless the deposited SiC material. As a consequence controlling and, next, lowering the residual strain appear of fundamental technical interest.

In this work we focus on the investigation of the residual strain (and strain relaxation) in the 3*C*-SiC/Si heteroepitaxial semiconductor system. We use micro-Raman spectroscopy as a probe and, to account for the asymmetric line shape experimentally observed, develop in full details a theoretical model which takes into account the finite effect of stress inhomogeneities near the interface. Finally, focusing on three 3*C*-SiC/Si samples coming from different origins, we show that every time the residual strain relaxes with an approximate z^{-1} dependence.

This paper is organized as follows. In Sec. II, we discuss the physics of probing the strain by Raman spectroscopy. We make clear the difference which does exist between the constant-strain approximation (which is the standard one, only considered in the literature up to now) and both the homogeneous and inhomogeneous strain approximations. These two complementary features where recently introduced[3] in order to take into account the spatial fluctuations which generally exist in the bulk of any epitaxial layer and *a fortiori* close to the interfaces. In Sec. III, we recapitulate the motion equation of optical phonons in the long-wave approximation including the strain (Sec. III A) while, in Sec. III B, the Green's functions method is applied to consider the effect of the strain fluctuations in very much detail. We obtain the inhomogeneous broadening and shift in terms of the strain correlation function. A Gaussian strain correlator is used (in Sec. III C) to perform final estimations. The Raman cross section is finally given in Sec. III E, where the selection rules are discussed. The comparison with experimental data for 3*C*-SiC deposited on silicon is given in Sec. IV. We show that, in this particular material system where the lattice mismatch between SiC and Si is about 20%, there exist both homogeneous strain with a smooth relaxation and a noticeable inhomogeneous contribution to the Raman spectra. Performing a detailed comparison between the theoretical pre-

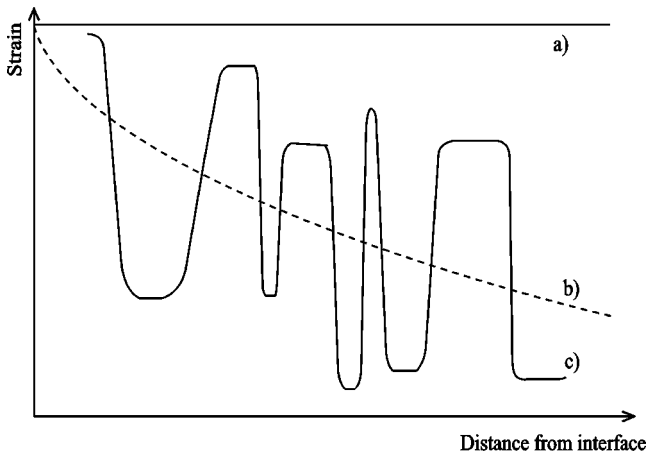

FIG. 1. Schematic drawing of the various strain distributions encountered near two semiconductors heterointerfaces: (a) a constant strain which corresponds with the standard approximation for bulk material, (b) a smoothly relaxing term, and (c) a fluctuating, nonhomogeneous, component.

dictions and the experimental data, we find that the inhomogeneous contribution can be either short range, for a three-dimensional growth-type material, or long-range, for better optimized (more two-dimensional) growth conditions and post-grown annealed samples.

II. PROBING THE STRAIN RELAXATION BY RAMAN SPECTROSCOPY

From the experimental point of view, Raman scattering is by far one of the most popular techniques to investigate the residual strain, both in bulk materials and in multilayered semiconductor structures. However, only the line shift resulting from the uniform strain approximation [see Fig. 1(a)] has been investigated in detail.[4,5].

In many cases this approach is far from sufficient, both from the experimental and theoretical point of view. For instance, the strain induced by the differences of lattice constants and thermal coefficients between two adjacent layers is known to relax when moving from the interface to the free surface. This is shown along the z direction in Fig. 1(b). Because such a strain changes its value on a large scale one can observe the smooth strain variation in an heteroepitaxial material system, by displacing a laser spot on the lateral surface (on both parts of the interface) and by measuring the phonon line shift $\Delta\omega^{(\mathrm{un})}$. Typical results have been reported in Ref. 6. We call this effect *the uniform shift*.

Of course, since there are different layers in the laser spot with different strain values, the uniform strain relaxation must result in a finite Raman linewidth, $\Gamma^{(\mathrm{un})} = d\partial(\Delta\omega^{(\mathrm{un})})/\partial z$, where d is the laser spot diameter. Typically since the strain relaxes over distances $\sim 10\ \mu$m and induces a line shift $\Delta\omega^{(\mathrm{un})} \sim 2\ \mathrm{cm}^{-1}$, using the experimental resolution $d \simeq 1\ \mu$m and the uniform shift approximation, one finds a broadening $\Gamma^{(\mathrm{un})} \sim 0.2\ \mathrm{cm}^{-1}$. This is negligible in comparison with the experimental linewidth, which is usually of the order of several cm^{-1}.

We have recently shown (see Ref. 3) that the strain fluctuations located near a semiconductor heterointerface also lead to a broadening (and shift) of the Raman lines. This is a very large effect which comes because the strain fluctuations destroy the perfect lattice symmetry and allow a coupling of phonon states with different k values. In this work we show that, every time, the strain consists of a spatial fluctuating component superimposed on the term which reduces smoothly in real space [Fig. 1(c)]. Such strain fluctuations result from dislocations, grain or twin structures, and other structural defects.

In the backscattering geometry, according to the standard momentum conservation law, an optical phonon excited by light has twice the momentum of the incident photon and ''sees'' the smooth strain averaged over distances of the order of the collecting spot. This is typically of the order of the light wavelength, which is large in the interatomic scale. Performing such an average, we obtain (besides the smooth strain) the effect of the fluctuating strain in the second order of the perturbation theory. We show that the fluctuating strain induces both *an inhomogeneous broadening* $\Gamma^{(\mathrm{inh})}$ and *a shift* $\Delta\omega^{(\mathrm{inh})}$ of the Raman line. To the best of our knowledge, the influence of such a disorder on the Raman modes has never been considered up to now (either for the TO or LO component), even if it is absolutely necessary in order to get a clear understanding of the strain relaxation near two semiconductor heterointerfaces.

From the theoretical point of view, this problem has two peculiar features. First, because of the small uniform splitting of the normally degenerated phonons, interbranch phonon scattering becomes allowed. Of course, this scattering is driven by the static strain fluctuations. Second, the momentum transfer from the light to phonons remains relatively small. Then one has to calculate the phonon shift and width near the extrema of the optical phonon branches. We will see that the inhomogeneous shift and width have singularities at the top of the branches. As a result, the shift and width become frequency dependent. Therefore, the phonon mode acquires an asymmetric line shape.

This asymmetry has no relation to the so-called Fano interference effect, which is also known as the Breit-Wigner resonance in nuclear physics. Indeed, starting from the most general viewpoint, Raman spectra result from a very complex picture of a photon-electron-phonon interaction (even if full attention to their very subtle aspects has only been paid recently). It was first discovered that the interaction of the phonon resonance with the electron-hole continuum can lead to characteristic changes in the shape of the resonance line. Concerning SiC, this Fano interference effect was discussed for n-type 6H SiC in Ref. 7 and, more recently, in Ref. 8 for 4H and 6H polytypes. Another example of this behavior is the asymmetric 340 cm^{-1} line in superconducting YBaCuO. It has been discussed several times in the literature[9–11] and is currently considered as an important probe of the electron-phonon interaction in this prototype superconducting compound.

Since the phonon Raman scattering is determined by the phonon Green's function averaged over the static strain fluctuations, we write the appropriate Dyson's equation for the Green's function considering the interaction of phonons with the strain fluctuations. Then the integral equations for the width and shift, which are functions of the frequency transfer, are solved self-consistently. We find the inhomogeneous broadening and shift in terms of the strain correlation func-

tion and, using the obtained width and shift, we calculate the Raman line shape.

The proposed theory is very similar to the theory of the conductivity of metals with impurities, but the effect of branch extrema is essential. Our method can be applied to the scattering of optical phonons by imperfections (and other problems) if the momentum transfer Δk is comparable to the value determined by the collision rate. This problem has physical significance due to a small value of the dimensionless parameter $a\Delta k \simeq \sqrt{\Gamma/\omega_0} \ll 1$, where a is the lattice constant, $\Gamma \simeq 2-5\ \mathrm{cm}^{-1}$, and $\omega_0 \simeq 600-1000\ \mathrm{cm}^{-1}$ (these are typical values for the optical phonon width and frequency, respectively). We will see that the scale of fluctuations $r_0/a \simeq \sqrt{\omega_0/\Gamma}/\pi$ (i.e., moderately large in the atomic units a) is of special interest for the problem under consideration.

III. THEORY

A. Uniform strain

In the long-wavelength approximation, the equation of motion for the optical phonon displacements $u_i(r,\omega)$ can be written in the following form:

$$(H - i\omega\Gamma^{(\mathrm{int})} + V(\mathbf{r}) - \omega^2)u(\mathbf{r},\omega) = 0, \tag{1}$$

where the matrix elements

$$H_{ij} = \chi_{ij} + \mu_{ijlm}\frac{\partial^2}{\partial x_l \partial x_m} \tag{2}$$

represent the long-wave expansion of the dynamical matrix with constant tensors χ_{ij} and μ_{ijlm}. The damping $\Gamma^{(\mathrm{int})}$ describes the intrinsic phonon width caused by the phonon-phonon and electron-phonon interactions[12] and the matrix

$$V_{ij}(\mathbf{r}) = \lambda_{ijlm}\varepsilon_{lm}(\mathbf{r}) \tag{3}$$

takes into account the strain effect $\varepsilon_{lm}(\mathbf{r})$. Expression (3) is well known and was proposed initially[4] for the constant-strain approximation illustrated in Fig. 1(a).

In cubic crystals there are three optical phonons at the Γ point, with a threefold degenerate frequency ($i=1$–3). Then, the tensor χ_{ij} has only diagonal elements $\chi_{ij} = \omega_0^2\delta_{ij}$ and both $\lambda_{ijlm} \simeq \omega_0^2$ and μ_{ijlm} have three independent components (e.g., $\lambda_{xxxx} = p$, $\lambda_{xxyy} = q$, and $\lambda_{xyxy} = r$). The long-range Coulomb forces further split the degeneracy of the optical phonons in such a way that the LO phonon has a higher frequency than the twofold degenerate TO phonon. Let us emphasize that $\chi_{ij} = 0$ for the acoustic phonons. This gives the linear dispersion near $k=0$, instead of the quadratic one for optical phonons. The tensor μ_{ijlm} has the same order of magnitude for both the acoustic and optical modes ($\mu_{ijlm} \simeq s^2$, where s is the sound velocity). This comes simply because, if one extrapolates any acoustic branch to the boundary of the Brillouin zone, one obtains a typical frequency (ω_0) of the order of magnitude of the value of optical phonons. The typical value of μ for the axial k direction in SiC may be estimated using well-known data for the upper optical mode:[13] $\omega = 970\ \mathrm{cm}^{-1}$ at $k=0$ and $\omega = 885\ \mathrm{cm}^{-1}$ at $k/k_{\max} = 0.67$, where $k_{\max} = 6\pi/c$ and the axial dimension of the unit cell $c = 15.12$ Å. One obtains $\sqrt{\mu} = 0.9 \times 10^6$ cm/s.

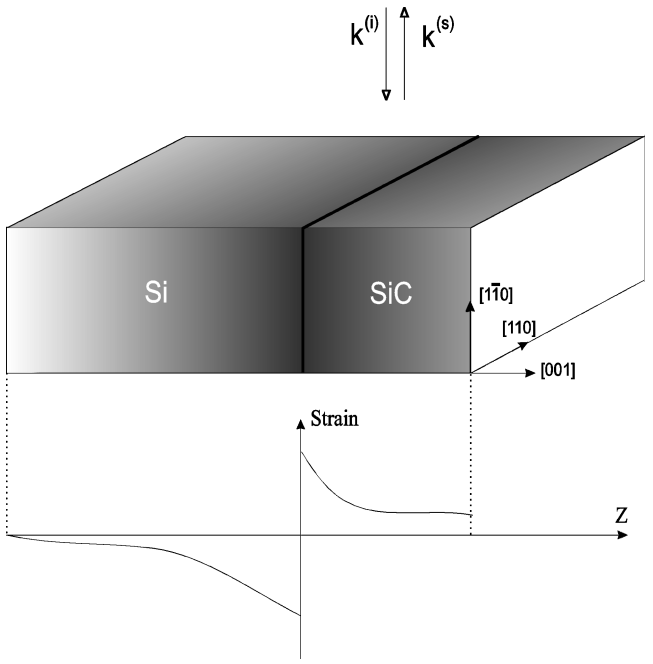

FIG. 2. Schematic drawing of the Raman backscattering geometry used in this work to investigate the strain relaxation at the 3C-SiC/Si interface. Both the incident and scattered light propagate parallel to the $\langle 1\,\bar{1}\,0\rangle$ direction. The strain relaxation is probed by displacing the laser spot in the $\langle 001\rangle$ direction.

The Raman cross section is obtained using the Green's functions of the optical phonons $D_{ij}(\mathbf{r},\mathbf{r}',\omega)$ for which we have the equation

$$[H - i\omega\Gamma^{(\mathrm{int})} + V(\mathbf{r}) - \omega^2]D(\mathbf{r},\mathbf{r}',\omega) = \delta(\mathbf{r}-\mathbf{r}'), \tag{4}$$

where the Green's functions have to be averaged as previously described. Using the diagram technique and summing diagrams with the averaged $\langle V\rangle$, we get

$$\langle D(\mathbf{r},\mathbf{r}',\omega)\rangle = D^{(0)}(\mathbf{r}-\mathbf{r}',\omega) = \int \frac{d^3k}{(2\pi)^3} D^{(0)}(\mathbf{k},\omega)e^{i\mathbf{k}(\mathbf{r}-\mathbf{r}')},$$

where

$$D^{(0)-1}(\mathbf{k},\omega) = H(\mathbf{k}) - i\omega\Gamma^{(\mathrm{int})} + \langle V(\mathbf{r})\rangle - \omega^2. \tag{5}$$

The matrix elements are $H_{ij} = \chi_{ij} - \mu_{ijlm}k_l k_m$ and $\langle V_{ij}(\mathbf{r})\rangle = \lambda_{ijlm}\langle\varepsilon_{lm}(\mathbf{r})\rangle$. The symmetry of the averaged $\langle\varepsilon_{ij}\rangle$ is determined by the experimental conditions.

If a twofold symmetry is preserved in the plane parallel to the interface (see Fig. 2), then $\langle\varepsilon_{xx}\rangle = \langle\varepsilon_{yy}\rangle = \varepsilon_\parallel$, $\langle\varepsilon_{zz}\rangle = \varepsilon_\perp$, and $\langle\varepsilon_{xz}\rangle = \langle\varepsilon_{yz}\rangle = \varepsilon_\Delta$. As a consequence, for phonons propagating in the plane $k_z = 0$, the matrix $H + \langle V\rangle$ has only the following five components:

$$H_{xx} + \langle V_{xx}\rangle = \omega_0^2 + (p+q)\varepsilon_\parallel + q\varepsilon_\perp - \mu_{xxxx}k_x^2 - \mu_{xxyy}k_y^2,$$

$$H_{yy} + \langle V_{yy}\rangle = \omega_0^2 + (p+q)\varepsilon_\parallel + q\varepsilon_\perp - \mu_{xxxx}k_y^2 - \mu_{xxyy}k_x^2,$$

$$H_{zz} + \langle V_{zz}\rangle = \omega_0^2 + 2q\varepsilon_\parallel + p\varepsilon_\perp - \mu_{xxyy}k^2,$$

$$H_{xy} + \langle V_{xy}\rangle = -2\mu_{xyxy}k_x k_y,$$

$$H_{xz} + \langle V_{xz}\rangle = H_{yz} + \langle V_{yz}\rangle = 2r\varepsilon_\Delta. \tag{6}$$

In the case of backscattering from a $\{1\,\bar{1}\,0\}$ face (see Fig. 2), it is useful to turn the coordinate axes in the xy plane in such a way that $x=(x'-y')/\sqrt{2}$ and $y=(x'+y')/\sqrt{2}$ (i.e., choosing x' along the light propagation and parallel to the momentum transfer). Then the matrix (6) has only two nonzero off-diagonal matrix elements $\langle V_{x'z}\rangle=\langle V_{zx'}\rangle=2\sqrt{2}r\varepsilon_\Delta$ which connect the LO(x') and TO(z) modes.

Let us consider the particular case of SiC. The Coulomb splitting $\omega_{\rm LO}-\omega_{\rm TO}\simeq 100\ {\rm cm}^{-1}$. Then, in comparison to $\langle V\rangle$, the contribution of $\langle V_{x'z}\rangle$ to the shift of the LO(x') and TO(z) phonons is $\delta\omega/\langle V\rangle\sim\langle V_{x'z}\rangle^2/\varepsilon\omega_0^2(\omega_{\rm LO}^2-\omega_{\rm TO}^2)\sim\varepsilon\omega_0^2/(\omega_{\rm LO}^2-\omega_{\rm TO}^2)$. As an order of magnitude, we take $p\sim q\sim r\sim\omega_0^2$ and $\varepsilon_{ij}\sim\varepsilon$. Moreover, in the case under consideration the frequencies of optical phonons $\omega_0\sim 10^3\ {\rm cm}^{-1}$. Finally, from our experimental data, we estimate $\varepsilon\sim 10^{-3}$ in accordance with Ref. 14. Altogether, this shows that one can safely omit $\langle V_{x'z}\rangle$. In this approximation, the matrix (6) has a diagonal form with three nondegenerate eigenvalues:

$$\omega_{\rm LO}^{(x')}=\omega_{\rm LO}^{(0)}+[(p+q)\varepsilon_\parallel+q\varepsilon_\perp -(\mu_{xxxx}+\mu_{xxyy}+2\mu_{xyxy})k^2/2]/2\omega_0,$$

$$\omega_{\rm TO}^{(y')}=\omega_0+[(p+q)\varepsilon_\parallel+q\varepsilon_\perp -(\mu_{xxxx}+\mu_{xxyy}-2\mu_{xyxy})k^2/2]/2\omega_0,$$

$$\omega_{\rm TO}^{(z)}=\omega_0+(2q\varepsilon_\parallel+p\varepsilon_\perp-\mu_{xxyy}k^2)/2\omega_0, \tag{7}$$

where the superscripts x', y', and z denote the phonon polarization, and $\omega_{\rm LO}^{(0)}$ differs from ω_0 because of the Coulomb forces.

We see immediately from Eqs. (7), that both the LO(x') and TO(y') phonons must have the same uniform strain shift,

$$\Delta\omega_{x'}^{(\rm un)}=\Delta\omega_{y'}^{(\rm un)}=[(p+q)\varepsilon_\parallel+q\varepsilon_\perp]/2\omega_0, \tag{8}$$

while the TO(z) phonon shift will manifest, as a function of strain, a different slope:

$$\Delta\omega_z^{(\rm un)}=(2q\varepsilon_\parallel+p\varepsilon_\perp)/2\omega_0.$$

Let us apply the preceding results (7) to $3C$-SiC/Si in the case of the geometry shown in Fig. 2. On the SiC side, the Coulomb forces split the optical triplet into a singlet LO(x') and a doublet TO(y') and TO(z). This doublet is further split by strain and, among the three components, two phonon branches [LO(x') and TO(y')] must experience an identical strain dependence. In other words their frequencies must decrease in the same manner under the effect of the tensile strain components which originate from the interfacial SiC/Si lattice mismatch. On the Si side, the strain will be compressive and no Coulomb forces will exist. Therefore, the optical triplet will be only split by strain in a singlet TO(z) and a doublet LO(x'), TO(y'). We do not write the obvious result which can be easily obtained solving the secular equation with the matrix elements (6) and taking into account $\langle V_{x'z}\rangle$.

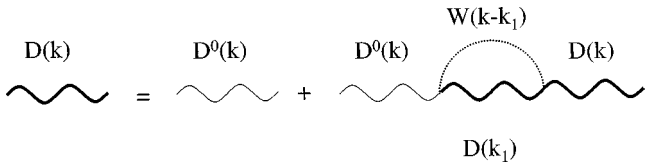

FIG. 3. Dyson's equation for the averaged phonon Green's function (wave line). The strain correlation function is shown by the dotted line.

B. Inhomogeneous broadening in the Born approximation

Let us now consider the effect of the strain fluctuations $\delta V(\mathbf{r})=V(\mathbf{r})-\langle V(\mathbf{r})\rangle$ shown in Fig. 1(c). Summing again the important diagrams with the correlator $\langle\delta V\delta V\rangle$ (see Ref. 3), we get the averaged solution of Eq. (4) shown in Fig. 3. This solution depends on the coordinates difference $\mathbf{r}-\mathbf{r}'$ and, for its Fourier transform, we obtain the Dyson's equation

$$D_{ij}^{-1}(\mathbf{k},\omega)=D_{ij}^{(0)-1}(\mathbf{k},\omega)-\int\frac{d^3k_1}{(2\pi)^3}W_{imlj}(\mathbf{k}_1-\mathbf{k})\times D_{ml}(\mathbf{k}_1,\omega), \tag{9}$$

where the matrix $D_{ij}^{(0)}(\mathbf{k},\omega)$ is given in Eqs. (5) and (6) and $W_{imlj}(\mathbf{k})$ is the Fourier transform of the correlation function:

$$W_{imlj}(\mathbf{r}-\mathbf{r}')=\langle\delta V_{im}(\mathbf{r})\,\delta V_{lj}(\mathbf{r}')\rangle.$$

The matrix $D^{(0)}$ is diagonal in our case [see Eq. (7)]. Moreover in the Born approximation, if the effect of fluctuations is comparatively small, one can take $D^{(0)}$ in the integrand instead of D. Then one obtains for the diagonal elements the expression

$$D_{jj}(\mathbf{k},\omega)^{-1}=D_{jj}^{(0)}(\mathbf{k},\omega)^{-1}-\sum_m\int\frac{d^3k_1}{(2\pi)^3}W_{jmmj}(\mathbf{k}_1-\mathbf{k})\times D_{mm}^{(0)}(\mathbf{k}_1), \tag{10}$$

which has a transparent meaning. In the absence of disorder, the poles of $D_{jj}^{(0)-1}(\mathbf{k},\omega)$, Eq. (5), give the phonons dispersion law, Eqs. (7) and (8):

$$\omega_j^2(k)=\omega_j^2(k=0)-s_j^2k^2-i\omega\Gamma_j^{(\rm int)},$$

where the parameters s_j are of order of the sound velocity and depend on the $\mathbf{k}$ direction (we will neglect this dependence). The uniform shift is included in $\omega_j^2(k=0)$.

In the limiting case $\Gamma^{(\rm int)}\to 0$, the imaginary part of integral (10),

$$\omega\Gamma_j^{(\rm inh)}(\mathbf{k},\omega)=\pi\sum_m\int\frac{d^3k_1}{(2\pi)^3}W_{jmmj}(\mathbf{k}_1-\mathbf{k})\times\delta(\omega_m^2(\mathbf{k}_1)-\omega^2), \tag{11}$$

and the real part

$$2\omega_0\Delta\omega_j^{(\rm inh)}(\mathbf{k},\omega)=\sum_m\int\frac{d^3k_1}{(2\pi)^3}\frac{W_{jmmj}(\mathbf{k}_1-\mathbf{k})}{\omega^2-\omega_m^2(\mathbf{k}_1)} \tag{12}$$

give the phonon inhomogeneous broadening and shift, respectively.

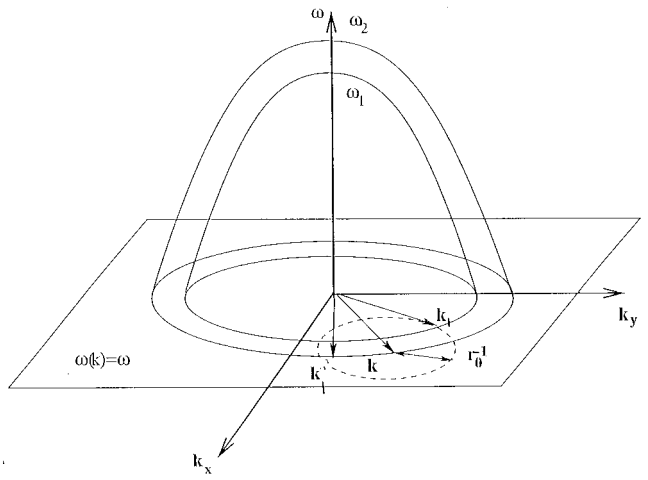

FIG. 4. Mechanisms of intraband and interband phonon scattering induced by the strain fluctuations considered in this work. The two optical phonon branches $\omega_{1,2}(\mathbf{k})$ are shown near maximum. All possible transitions are from an initial state $(\omega,\mathbf{k})$ to a final state $(\omega,\mathbf{k}_1)$ which belongs to the domain of radius r_0 where the strain correlation function does not vanish.

Equation (11) has the form of the ''golden'' rule, while Eq. (12) reminds us of the formula of the second-order perturbation theory. Let us remark that the Dirac δ function in Eq. (11) expresses the phonon energy conservation law in the scattering process by static fluctuations. Then the transition from a state $(\mathbf{k},\omega)$ is possible only to states with different $\mathbf{k}_1$ values but with the same final energy $\omega_m(\mathbf{k}_1)=\omega$. Thus the correlator $W_{jmmj}(\mathbf{k}_1-\mathbf{k})$ has then the meaning of a transition probability $(j,\mathbf{k})\rightarrow(m,\mathbf{k}_1)$.

To make an estimate, we approximate the correlator by a Gaussian function

$$W_{imlj}(\mathbf{r}-\mathbf{r}')=\varepsilon^2\omega_0^4 w_{imlj}e^{-(\mathbf{r}-\mathbf{r}')^2/2r_0^2}, \tag{13}$$

where the prefactor is inserted to use a dimensionless parameter w which does not depend (in the leading approximation) on the value of the average strain. This is the mean-squared fluctuation at point $\mathbf{r}$, divided by the squared mean strain and the phonon frequency to the fourth power. The correlation radius r_0 defines the average domain size where a strain of order of the mean value exists. The Fourier transform of expression (13) gives then

$$W_{imlj}(\mathbf{k})=\int d^3r e^{-i\mathbf{k}\cdot\mathbf{r}}W_{imlj}(\mathbf{r}) =(2\pi)^{3/2}\varepsilon^2\omega_0^4 r_0^3 w_{imlj}e^{-k^2r_0^2/2}. \tag{14}$$

In Fig. 4, two phonon bands $\omega_{1,2}(\mathbf{k})$ have been drawn schematically (the vector $\mathbf{k}$ being, of course, three dimensional) and we assume that both branches have a maximum at $k=0$. A phonon with momentum $\mathbf{k}$ and frequency $\omega=\omega_1(\mathbf{k})$ can be scattered into states with momentum $\mathbf{k}_1$ and frequency $\omega_1(\mathbf{k}_1)=\omega$ (intraband transition) or with frequency $\omega_2(\mathbf{k}_1)=\omega$ (interband transition). The ω plane in $\mathbf{k}$ space is shown for the case $\omega^2<\omega_1^2(k=0)<\omega_2^2(k=0)$. The only region into which the transitions are possible (i.e., where the correlator does not vanish) is shown by a dotted circle of radius r_0^{-1}. If $\omega^2>\omega_1^2(k=0)$, the intraband transitions are not allowed.

C. Inhomogeneous broadening near the top of phonon branches

If the width Γ is large, one cannot use the δ function in Eq. (11) but, instead, one should hold Γ in the integrand. Transforming Eq. (9) to the diagonal form, we search for the solution

$$D_{jj}^{-1}(\mathbf{k},\omega)=\omega_j^2(\mathbf{k},\omega)-s_j^2k^2-i\omega\Gamma_j(\mathbf{k},\omega)-\omega^2, \tag{15}$$

where $\omega_j(\mathbf{k},\omega)=\omega_j(k=0)+\Delta\omega_j^{(\mathrm{inh})}(\mathbf{k},\omega)$ and $\Gamma_j(\mathbf{k},\omega)=\Gamma_j^{(\mathrm{int})}+\Gamma_j^{(\mathrm{inh})}(\mathbf{k},\omega)$. Substituting Eq. (15) in Eq. (9) and taking the imaginary and real parts, we get for the inhomogeneous broadening $\Gamma_j^{(\mathrm{inh})}(\mathbf{k},\omega)$ and shift $\Delta\omega_j^{(\mathrm{inh})}(\mathbf{k},\omega)$ the following system of coupled integral equations:

$$\Gamma_j^{(\mathrm{inh})}(\mathbf{k},\omega) =\sum_m\int\frac{d^3k_1}{(2\pi)^3} \times\frac{\Gamma_m(\mathbf{k}_1,\omega)W_{jmmj}(\mathbf{k}_1-\mathbf{k})}{[\omega_m^2(\mathbf{k}_1,\omega)-\omega^2-s_m^2k_1^2]^2+[\omega\Gamma_m(\mathbf{k}_1,\omega)]^2}, \tag{16}$$

$$\Delta\omega_j^{(\mathrm{inh})}(\mathbf{k},\omega) =\sum_m\int\frac{d^3k_1}{(2\pi)^3 2\omega_0} \times\frac{[\omega^2-\omega_m^2(\mathbf{k}_1,\omega)+s_m^2k_1^2]W_{jmmj}(\mathbf{k}_1-\mathbf{k})}{[\omega_m^2(\mathbf{k}_1,\omega)-\omega^2-s_m^2k_1^2]^2+[\omega\Gamma_m(\mathbf{k}_1,\omega)]^2}. \tag{17}$$

The right-hand sides of Eqs. (16) and (17) contain the total damping $\Gamma_m(\mathbf{k}_1,\omega)=\Gamma_m^{(\mathrm{int})}+\Gamma_m^{(\mathrm{inh})}(\mathbf{k}_1,\omega)$ and the total shift $\omega_m(\mathbf{k}_1,\omega)=\omega_m(\mathbf{k}_1=0)+\Delta\omega_m^{(\mathrm{inh})}(\mathbf{k}_1,\omega)$. The uniform shift $\Delta\omega_m^{(\mathrm{un})}$, Eqs. (7) and (8), is included in $\omega_m(\mathbf{k}_1=0)$.

Performing the integrals (16) and (17), we need to take into account the band edges. The momentum $\mathbf{k}$ and frequency ω in Eqs. (16) and (17) have the sense of a momentum and frequency transfer for the light scattering. In the optical range, $k\sim10^5$ cm^{-1}. The frequencies and damping of the optical phonons in Si and SiC are $\omega_0\simeq600$–1000 cm^{-1} and $\Gamma\simeq2$–5 cm^{-1}, respectively; the dispersion parameter $s\simeq10^6$ cm/s. Therefore, the condition $sk\ll\sqrt{\omega_0\Gamma}$ is valid in all experimental cases discussed below. In these conditions $\Gamma_j^{(\mathrm{inh})}(\mathbf{k},\omega)$ and $\Delta\omega_j^{(\mathrm{inh})}(\mathbf{k},\omega)$ can be regarded as independent of $\mathbf{k}$. Concerning $\mathbf{q}=\mathbf{k}_1-\mathbf{k}$, the values $q^2\leqslant2/r_0^2$ determine the final states (shown in Fig. 4 by a dotted circle) for phonons scattered by the strain fluctuations. The domain $q^2\leqslant\omega_0\Gamma/s^2$ is essential in the integrand Green's function D [see Eq. (15)]. This is because we are interested in $|\omega_j-\omega|\simeq\Gamma$. Depending on either the parameter $\pi\sqrt{\Gamma/\omega_0}r_0/a$ being small or large ($a\simeq\pi s/\omega_0$ being the lattice parameter), we

see that two limiting cases are possible. Then all integrals can be done analytically and a system of algebraic equations is found.

Let us emphasize that the value $\sqrt{\omega_0/\Gamma}/\pi$ is moderately large. This means that the condition of validity of the present theory (which is defined by the crossover value $r_0/a = \sqrt{\omega_0/\Gamma}/\pi$) is indeed satisfied. It means that the radius of strain imperfections is moderately large in atomic units, which is the basis for achieving a good physical significance of the present results.

Consider now the two limiting cases separately.

1. Correlation radius is small

In this case, $\pi[\max(\Gamma,|\omega_j-\omega|)]^{1/2}\omega_0^{-1/2}r_0/a \ll 1$, which means that $r_0/a<10$ for the set of parameters mentioned above. We first notice that, for such values of r_0/a, the suitable regions $|\omega_j-\omega|$ are narrow. In this case, when scattering on the strain fluctuations, the phonon may experience a considerable momentum change. As a consequence, in the convergent integral for the width, we take the correlator at $q=0$ and integrate over $\mathbf{k}_1$. In the same way, the leading contribution in the integral for the shift comes from the large values $q[\omega_0\max(\Gamma,|\omega_j-\omega|)/s^2<q^2<2/r_0^2]$, where the width and shift are not important. The next term (in which the exponent can be omitted) should be held, since it depends on ω. Then, Eqs. (16) and (17) read

$$\Gamma_j^{(\mathrm{inh})}(\omega)=\omega_0\sum_m \frac{v_{jm}\Gamma_m(\omega)}{|\omega_m^2-\omega^2|^{1/2}} \times\int_0^\infty \frac{x^2dx}{[\theta(\omega_m^2-\omega^2)-x^2]^2+\gamma_m^2(\omega)}, \quad (18)$$

$$\Delta\omega_j^{(\mathrm{inh})}(\omega)=\frac{1}{2}\sum_m v_{jm}|\omega_m^2-\omega^2|^{1/2} \times\int_0^\infty \frac{e^{-x^2/x_m^2}[\theta(\omega_m^2-\omega^2)-x^2]x^2dx}{[\theta(\omega_m^2-\omega^2)-x^2]^2+\gamma_m^2(\omega)}, \quad (19)$$

where

$$v_{jm}=\sqrt{\frac{2}{\pi}}\varepsilon^2\left(\frac{\omega_0 r_0}{s_m}\right)^3 w_{jmmj}\simeq\sqrt{\frac{2}{\pi}}\varepsilon^2\left(\frac{\pi r_0}{a}\right)^3 w_{jmmj},$$

$$\gamma_m(\omega)=\frac{\omega\Gamma_m(\omega)}{|\omega_m^2-\omega^2|},$$

$$x_m=\frac{s_m}{r_0}\frac{\sqrt{2}}{|\omega_m^2-\omega^2|^{1/2}}\simeq\frac{a}{\pi r_0}\frac{\omega_0^{1/2}}{|\omega_m-\omega|^{1/2}}, \quad (20)$$

$\theta(\omega_m^2-\omega^2)$ is the unit step Heaviside function, and $v_{jm}>0$. For simplicity, we omit the argument ω in $\omega_m(\omega)$.

Performing the integrals,

$$\int_0^\infty \frac{x^2dx}{(\theta-x^2)^2+\gamma^2}=\frac{\pi}{2^{3/2}\gamma}[\theta+(\theta^2+\gamma^2)^{1/2}]^{1/2},$$

$$\int_0^\infty dx\frac{x^2(x^2-\theta)}{(\theta-x^2)^2+\gamma^2}e^{-x^2/x_m^2} =\frac{\sqrt{\pi}}{2}x_m-\frac{\pi}{2^{3/2}}[-\theta+(\theta^2+\gamma^2)^{1/2}]^{1/2}, \quad (21)$$

we obtain instead of Eqs. (18) and (19) a system of coupled algebraic equations for $\Gamma_j^{(\mathrm{inh})}(\omega)$ and $\Delta\omega_j^{(\mathrm{inh})}(\omega)$.

Let us consider the upper LO-phonon branch ($\omega^2\sim\omega_{\mathrm{LO}}^2$) in SiC, for which the intraband transitions are only possible. Then the subscripts in s_j,Γ_j, and w_{imlj} take only one value and we can omit them. Using Eqs. (21) and (20), we rewrite the system (18) and (19) in the form

$$\Gamma^{(\mathrm{inh})}(\omega)=(A/\omega_0)^{1/2}\{\omega_{\mathrm{LO}}^2-\omega^2+[(\omega^2-\omega_{\mathrm{LO}}^2)^2+\omega^2\Gamma^2]^{1/2}\}^{1/2}, \quad (22)$$

$$\Delta\omega^{(\mathrm{inh})}(\omega)=\left(\frac{A}{\omega_0}\right)^{1/2}\left(\frac{s}{\sqrt{\pi}r_0}-\frac{1}{2}\{-\omega_{\mathrm{LO}}^2+\omega^2+[(\omega^2-\omega_{\mathrm{LO}}^2)^2+\omega^2\Gamma^2]^{1/2}\}^{1/2}\right), \quad (23)$$

where the constant

$$A=\frac{\pi^2}{8}v^2\omega_0=\frac{\pi}{4}\omega_0\varepsilon^4\left(\frac{\omega_0 r_0}{s}\right)^6 w^2\simeq\frac{\pi}{4}\omega_0\varepsilon^4\left(\frac{\pi r_0}{a}\right)^6 w^2 \quad (24)$$

is related to the phonon scattering on strain fluctuations. For simplicity we omit the argument ω of functions $\Gamma(\omega)=\Gamma^{(\mathrm{int})}+\Gamma^{(\mathrm{inh})}(\omega)$ and $\omega_{\mathrm{LO}}(\omega)=\omega_{\mathrm{LO}}(k=0)+\Delta\omega^{(\mathrm{inh})}(\omega)$ [see definitions after Eq. (15)].

The numerical solutions of the coupled system (22) and (23) (the total width and inhomogeneous shift) as a function of the frequency transfer, together with $\mathrm{Im}D(\mathbf{k},\omega)$, have been already displayed at length in Ref. 3 for several values of the interaction constant A. They will not be repeated here.

The center of the line is determined by the equation $\omega_{\mathrm{LO}}(\omega)=\omega$ [see Eq. (15) with $k=0$] and using Eq. (22) one finds the total width at the center of line $\omega=\omega_{\mathrm{LO}}$:

$$\Gamma(\omega=\omega_{\mathrm{LO}})=\Gamma^{(\mathrm{int})}+A/2+[(A/2)^2+\Gamma^{(\mathrm{int})}A]^{1/2}. \quad (25)$$

Then, if the intrinsic width $\Gamma^{(\mathrm{int})}\ll A/4$, the total width reduces to

$$\Gamma(\omega=\omega_{\mathrm{LO}})=A+2\Gamma^{(\mathrm{int})}, \quad (26)$$

while, in the opposite case,

$$\Gamma(\omega=\omega_{\mathrm{LO}})=\sqrt{\Gamma^{(\mathrm{int})}A}+\Gamma^{(\mathrm{int})}. \quad (27)$$

One can see from Eqs. (26) and (27) that there exists an interference effect between the disorder width and the intrinsic collision rate—*they are not additive*. For the large strain fluctuations [see Eq. (26)], the intrinsic contribution is multiplied by a factor of 2, while in the opposite case [see Eq. 27)], the strain fluctuations involve a contribution proportional to the square root of the intrinsic width.

The width essentially depends on ω and increases below the top of the phonon branch. Far from the top, i.e., for $|\omega_{\mathrm{LO}}-\omega| \gg \Gamma/2$, we find

$$\Gamma(\omega) = \begin{cases} \Gamma^{(\mathrm{int})} + \sqrt{2A(\omega_{\mathrm{LO}}^2-\omega^2)/\omega_0} & \text{for } \omega_{\mathrm{LO}}^2-\omega^2 \gg \omega_0\Gamma, \\ \Gamma^{(\mathrm{int})}[1+\sqrt{A\omega_0/2(\omega^2-\omega_{\mathrm{LO}}^2)}] & \text{for } \omega^2-\omega_{\mathrm{LO}}^2 \gg \omega_0\Gamma, \end{cases} \tag{28}$$

which means clearly that the Raman line becomes asymmetric as soon as A becomes comparable to Γ. The explanation of this behavior is to be found in the LO-phonon density of states. It is equal to zero for $\omega^2 > \omega_{\mathrm{LO}}^2$ (if $\Gamma^{(\mathrm{int})} \to 0$) and proportional to $\sqrt{\omega_{\mathrm{LO}}^2-\omega^2}$ below the top of the branch. Then, for any phonon scattered by the strain fluctuation, the final density of states increases below the top and results in an increased inhomogeneous width: the resonance curve drops more slowly on the low-frequency side of the peak.

For the inhomogeneous shift of the line, one can hold only the leading first term in Eq. (23):

$$\Delta\omega^{(\mathrm{inh})}(\omega=\omega_{\mathrm{LO}}) = (A/\pi\omega_0)^{1/2} s/r_0, \tag{29}$$

but the influence of the second term remains substantial. This is because it moves in the opposite direction the high-frequency part of the resonance curve (i.e., from high to low frequency). Of course, in every case, the total inhomogeneous shift (23) increases with increasing value of the disorder parameter A.

Formulas (18) and (19) also apply [see Eq. (21)] to the optical phonon doublet (in SiC) and to the triplet modes (in Si) but, in this case, several constants v_{im} should appear instead of v. Let us now consider the case of a large correlation radius.

2. Correlation radius is large ($\pi\sqrt{\Gamma/\omega_0}\, r_0/a \gg 1$)

This corresponds to a long-range disorder and, consequently, a small-angle scattering of phonons by the strain fluctuations. In this case, it is more convenient to introduce the variable $\mathbf{q}=\mathbf{k}_1-\mathbf{k}$ in Eqs. (16) and (17). The correlator becomes a sharp function and the phonon Green's function in the integrand should be expanded in a power series of $\mathbf{q}$. The zeroth-order term gives the final result in Eq. (16) while, in Eq. (17), terms to the second order are needed. Indeed, since the correlator is an even function, the first-order term vanishes. Performing the integral

$$\int \frac{d^3q}{(2\pi)^3} q^2 W_{immi}(q) = 3\varepsilon^2 \frac{\omega_0^4}{r_0^2} w_{immi},$$

we rewrite Eqs. (16) and (17) as

$$\Gamma_i - \Gamma_i^{(\mathrm{int})} = \omega_0^4 \sum_m \frac{\tilde{v}_{im}\Gamma_m}{(\omega_m^2-\omega^2)^2+\omega^2\Gamma_m^2}, \tag{30}$$

$$\Delta\omega_i^{(\mathrm{inh})} = \frac{\omega_0^3}{2} \sum_m \tilde{v}_{im} \left[\frac{\omega^2-\omega_m^2}{(\omega_m^2-\omega^2)^2+\omega^2\Gamma_m^2} + 3\left(\frac{s_m}{r_0}\right)^2 \frac{\omega^2\Gamma_m^2-(\omega_m^2-\omega^2)^2}{[(\omega_m^2-\omega^2)^2+\omega^2\Gamma_m^2]^2} \right], \tag{31}$$

where $\tilde{v}_{im}=\varepsilon^2 w_{immi}$, and Γ_m and ω_m are functions of ω.

Again, examples of numerical solutions for the coupled system (30) and (31), which give the total width and the inhomogeneous shift as a function of frequency transfer together with the Raman cross section $\mathrm{Im}D(\mathbf{k},\omega)$, have been shown at length in Ref. 3.

Similar to the previous case, these equations can be solved analytically for the center of line position ($\omega=\omega_{\mathrm{LO}}$) and for the wings. This gives correspondingly

$$\Gamma = \Gamma^{(\mathrm{int})}/2 + [(\Gamma^{(\mathrm{int})}/2)^2 + B^2]^{1/2} \tag{32}$$

and

$$\Gamma = \Gamma^{(\mathrm{int})}\left(1 + \frac{B^2\omega_0^2}{(\omega_{\mathrm{LO}}^2-\omega^2)^2}\right), \tag{33}$$

where $B^2=\varepsilon^2\omega_0^2 w$. The important point is that, while the line shape is still non-Lorentzian, it appears much more symmetric than it was in the previous case of the short-range disorder.

The center line position is determined by the equation $\omega_{\mathrm{LO}}=\omega$, which shows that only the last term in Eq. (31) contributes to the line shift:

$$\Delta\omega^{(\mathrm{inh})}(\omega=\omega_{\mathrm{LO}}) = 1.5(sB/r_0\Gamma)^2/\omega_0 \simeq 1.5\omega_0(aB/\pi r_0\Gamma)^2, \tag{34}$$

where Γ is obtained from Eq. (32).

Coming again to the degenerate case, the splitting can be found easily with the help of Eq. (31). This gives for the doublet TO modes ($i=1,2$)

$$\Delta\omega_{12}^{(\mathrm{inh})} = \mp\frac{\tilde{v}_{12}}{2}\frac{\omega_0^2}{\omega_2-\omega_1}. \tag{35}$$

To conclude this section, let us emphasize the most significant differences which separate the two limiting cases. For the short-range disorder (Sec. III C 1), the line shape is asymmetric. This can be seen from Eq. (28). However, the asymmetry is smaller than the line shift due to the parameter $\pi\sqrt{\Gamma/\omega_0}\, r_0/a \ll 1$. In the degenerate case, the splitting is also smaller than the common shift. Both the shift and broading depend on the correlation radius. For the long-range disorder (Sec. III C 2), the line shape remains symmetric, but non-Lorentzian, and the top of the line becomes flat. In the degenerate case, both the broadening (32) and splitting (35) are independent of the correlation radius. Finally whatever is the type of disorder, in both cases, it raises the top of the phonon branches [see Eqs. (29) and (34)]. This is in very good agreement with standard quantum mechanics arguments. By contrast, because this is a first-order correction, the uniform shift $\Delta\omega^{(\mathrm{un})}$ has an indefinite sign [see Eqs. (7) and (8)].

D. Anisotropic two-dimensional disorder

We assumed so far that the disorder was isotropic. However, in the presence of a heterointerface, the strain correla-

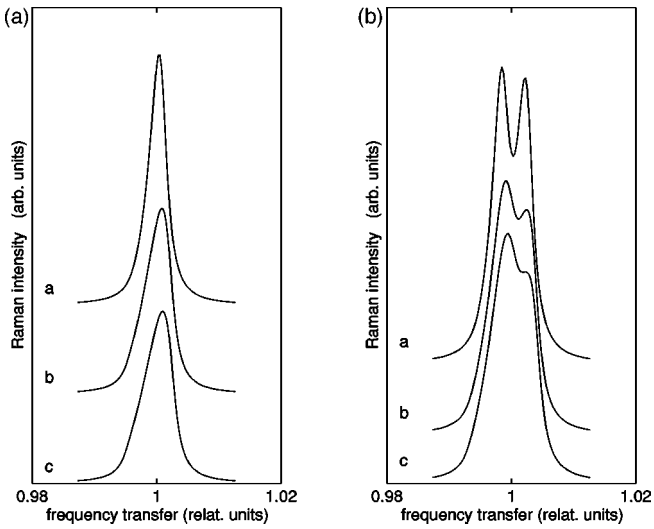

FIG. 5. Theoretical Raman intensity computed as a function of the frequency transfer for (a) a singlet and (b) a doublet mode in the case of a small correlation radius. The phonon transitions are possible into larger region than the one determined by the phonon width. The frequency transfer is measured in units of the phonon-mode frequency ω_0 (relative units). The intrinsic width $\Gamma^{(\mathrm{int})}/\omega_0 = 2.3\times 10^{-3}$. The correlation radius $r_0\omega_0/s = 20$. Finally, *a*, *b*, and *c* are for three values of the strain disorder. They give total widths $\Gamma/\omega_0 = 2.9$, 3.8, and 4.4×10^{-3}, respectively.

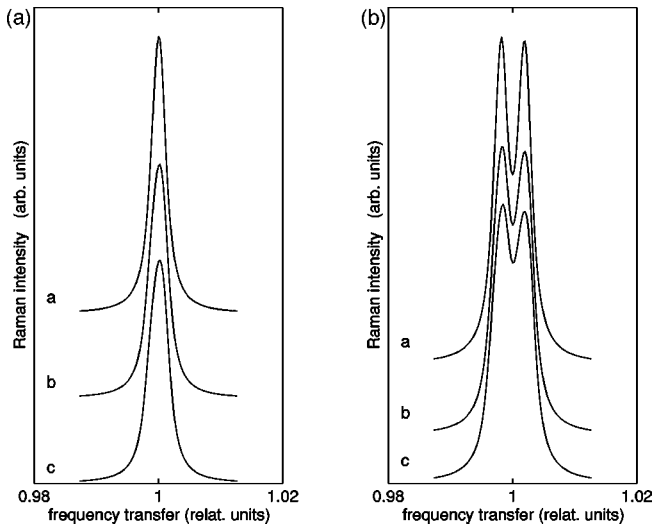

FIG. 6. Same as Fig. 5 but now in the case of a large correlation radius $r_0\omega_0/s = 40$.

tion function should have different behaviors in (at least) two different directions. One is perpendicular to the interface; the other one is tangent. As a consequence, we consider a prototype system with a large correlation radius in the normal z direction ($r_z/a \gg \sqrt{\omega_0/\Gamma}/\pi$), while making no assumption about the correlation radius r_0 for the directions parallel to the interface. For small values of the radius r_0 ($r_0/a \ll \sqrt{\omega_0/\Gamma}/\pi \ll r_z/a$), one can imagine this case like a set of columnar structures (or domains) growing perpendicular to the interface.

In the integral (9) with $k=0$, one can put $k_{1z}=0$ in $D_{ml}(\mathbf{k}_1,\omega)$. Then, omitting the exponent, the logarithmic integral over $k_{1\perp}$ can be done between the two limits 0 and $2s^2/r_0^2$. One obtains for the inhomogeneous width and shift of the phonon singlet

$$\Gamma^{(\mathrm{inh})}(\omega) = C\left[\arctan\left(\frac{\omega_{\mathrm{LO}}^2-\omega^2}{\omega\Gamma}\right) + \arctan\left(\frac{2s^2/r_0^2-\omega_{\mathrm{LO}}^2+\omega^2}{\omega\Gamma}\right)\right], \quad (36)$$

$$\Delta\omega^{(\mathrm{inh})}(\omega) = \frac{C}{4}\ln\frac{(2s^2/r_0^2+\omega^2-\omega_{\mathrm{LO}}^2)^2+\omega^2\Gamma^2}{(\omega^2-\omega_{\mathrm{LO}}^2)^2+\omega^2\Gamma^2}, \quad (37)$$

where $C=\varepsilon^2\omega_0^3 r_0^2 w/2s^2$.

For small values of the correlation radius r_0, the overall line shape remains asymmetric. This is shown in Fig. 5(a) for the LO singlet and in Fig. 5(b) for the TO doublet modes. In theses figures, three different values of the coupling constant have been used. They correspond to a small coupling (line *a*), an intermediate case of finite inhomogeneity (line *b*), and a strongly disordered system (line *c*). The striking point is that, in Fig. 5(b), the constant splitting of the two TO modes becomes more and more difficult to resolve because of the single line broadening, which increases rapidly from (a) to (c) [see Fig. 5(a)]. Performing a close comparison with the isotropic case of long-range disorder (see Sec. III C) we find that, in both cases, introducing a finite value of the coupling constant results in the appearance of a slowly decreasing low-energy tail. The main difference comes when comparing the high-energy one. It drops more slowly for the two-dimensional (2D) anisotropic case than it does for the isotropic one. This is because of the weaker dependence of the line shift coming from Eq. (37).

If r_0 is as large as r_z (i.e., satisfies the same condition), we come back to the long-range disorder case. In other words, we do not see any anisotropy anymore. Typical results are shown in Fig. 6. They concern both the LO singlet and TO doublet and, again, three different values of the coupling parameter have been considered. The striking point is that, even if non-Lorentzian, the overall line shape stays again much more symmetric than it was in the previous case of a small correlation radius. The direct consequence is a much better resolution of the TO doublet, especially in the case of the highest value of the coupling constant.

Finally, the conditions of validity for the basic equation (9) should be mentioned. The line shape on wings (28) and (33) can be obtained in the Born approximation (11) and (12). At the center of lines, the diagrams with intersections of the correlator lines make a contribution of the order of the diagram shown in Fig. 3 and a more sophisticated theory is needed. Then, one should consider Eq. (9) as a sensible interpolation between the two extreme limits.

E. Raman cross section

The effective Hamiltonian for the Raman scattering has the form

$$\hat{\mathcal{H}} = \frac{e^2}{mc^2}\int \frac{d^3k^{(s)}d^3k^{(i)}}{(2\pi)^6} g_{\alpha\beta\gamma}u_\alpha(\mathbf{k}^{(i)}-\mathbf{k}^{(s)})A_\beta(\mathbf{k}^{(i)})A_\gamma(\mathbf{k}^{(s)}), \quad (38)$$

where $A_\beta(\mathbf{k}^{(i)})$ and $A_\gamma(\mathbf{k}^{(s)})$ are the vector potentials of the incident and scattered light, respectively. The cross section for the light scattering into a solid angle $d\Omega^{(s)}$ and in the frequency interval $d\omega^{(s)}$, which is found by using the effective Hamiltonian (38), reads

$$\frac{d\sigma}{d\omega^{(s)}d\Omega^{(s)}}=\left(\frac{2e^2\omega^{(s)}}{c^2\hbar m\omega^{(i)}}\right)^2\frac{4/\pi}{1-\exp(-\hbar\omega/k_BT)}\times g_{\alpha\beta\gamma}e_\beta^{(i)}e_\gamma^{(s)}g_{\alpha'\beta'\gamma'}e_{\beta'}^{(i)}e_{\gamma'}^{(s)}\mathrm{Im}\,D_{\alpha\alpha'}(\mathbf{k},\omega), \tag{39}$$

where $e_\beta^{(i)}$ and $e_\gamma^{(s)}$ are polarization vectors.

Equation (39) shows that this is the imaginary part of the phonon Green's function which is measured in the Raman experiments. With respect to the interface, the parallel y' phonon is excited in the configuration $x'(zy')\overline{x'}$. It is still transverse, both in SiC and in Si, if the light beam makes a finite (small) angle with respect to the interface (the excited phonon has indeed the double momentum of incident and scattered light in the backscattering geometry). In the configuration $x'(y'y')\overline{x'}$ the z phonon is also excited. But if the incidence on the SiC side has a small angle with respect to the interface, this phonon has now a longitudinal component on the Si side. Therefore, the corresponding Raman line should be less intense than the corresponding y'-phonon mode. Finally, we can see from Eq. (38) that the longitudinal x' phonon should not be found when the light propagates in the x' direction; see Fig. 2. This is opposite to most experimental findings and we only see this forbidden phonon because the incident and collected light directions make a finite angle with the perfect x' direction. Of course, the scattered intensity is weak.

IV. COMPARISON WITH EXPERIMENTAL RESULTS

A. Samples and scattering geometry

We focused on three different 3C-SiC layers grown by CVD on ⟨100⟩-oriented silicon wafers. First was one sample obtained from CRHEA in Valbonne (France). Most details about the growth process can be found in Ref. 15 and only two points should be briefly outlined. First, the carbonization temperature was 1400 °C. Second, because the growth parameters are very difficult to stabilize in the long term, an *in situ* monitoring technique was used. This resulted in a rather homogeneous single crystal film, with about 18 μm in thickness, very well suited for investigation of the strain relaxation effects. The second sample was also noncommercial. It was 6 μm thick and obtained from LETI-CEA, in Grenoble (France). Full details about the growth technique and optimization of the buffer (carbonization) layer have been already given[16,17] and will not be repeated here. The main points are, first, a lower carbonization temperature (1200 °C, instead of 1400 °C in the case of the process used by CRHEA) and, second, a post-growth sacrificial oxidation that resulted in some improvement of the overall optical properties. Finally, a 3-μm-thick commercial 3C-SiC/Si sample was obtained from Cree Research Inc.[18]

Our Raman scattering experiments have been done at room temperature, on cleaved $\{1\,\bar{1}\,0\}$ sample surfaces. The sample geometry has already been described in Sec. II A and, for convenience, has been schematically drawn in Fig. 2. The excitation was provided by the Ar^+ 5145 Å line of a mixed argon-krypton ion laser. The scattered intensity was detected using a Jobin-Yvon T64000 spectrometer equipped with a cooled charge-coupled diode (CCD) camera. Because of the high sensitivity of the detection, we could perform reasonably fast measurements using a low-power excitation intensity. Usually, less than 500 μW incident power was focused on the sample.

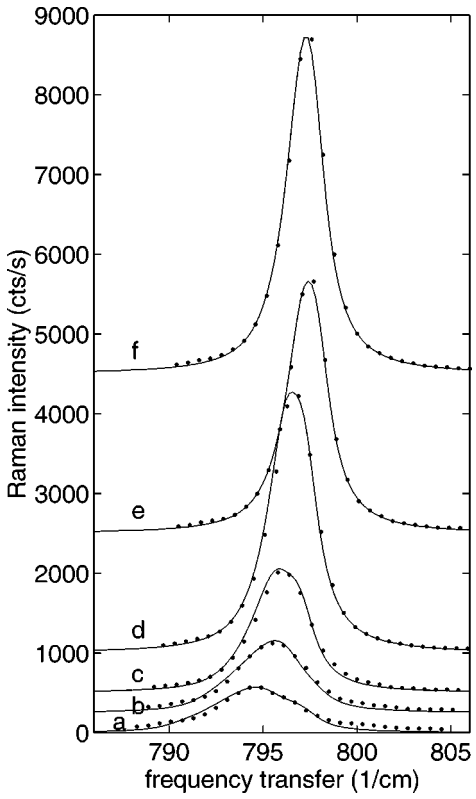

FIG. 7. Experimental Raman spectra (TO modes) collected on a 18-μm-thick 3C-SiC layer deposited on silicon. Starting from the interface (line a), two components resolve up to 0.5 μm (line b). The solid lines are fits to Eqs. (36) and (37). The intrinsic width is 1.8 cm^{-1} for all lines; the correlation radius $r_0\omega_0/s=20$. All remaining fitting parameters are listed in Table I.

As already discussed (see Sec. III E), using a confocal microscope both the incidence and collection angles are wide. This allows a finite departure from the perfect selection rules but, at the same time, defines a reasonably good backscattering configuration. Moreover, this ensures a spot size dimension (spatial resolution) of the order of 1 μm. Then, because of this high (spatial) resolution, one can easily move the laser beam on the cleaved $\{1\,\bar{1}\,0\}$ surface along the ⟨001⟩ direction. In this way, focusing at finite distances from the 3C-SiC/Si interface, we could collect different spectra at different (residual) strain magnitudes.

B. Strain-induced splitting of the TO modes

We consider, first, the thick sample from CRHEA and the experimental results displayed in Fig. 7. From bottom to top, the six different spectra correspond to six different spot positions on the surface (cleaved edge) of the sample. First, line

TABLE I. Final values (cm^{-1}) obtained in this work for the line position, width, and fitting parameters in the case of the $3C$-SiC/Si sample from CRHEA (see experimental spectra displayed in Fig. 7). Only the uniform shift is included in $\omega_{1,2}(0)$. The final line position and the width (at the center of the line) which result from strain fluctuations have been denoted $\omega_{1,2}(c)$ and $\Gamma_{1,2}(c)$, respectively. The adjusted coupling parameters C_{11}, C_{22}, and C_{12} are listed in the last column.

Distance from interface (μm)	TO1 line $\omega_1(0),\omega_1(c)$	Total $\Gamma_1(c)$	TO2 line $\omega_2(0),\omega_2(c)$	Total width $\Gamma_2(c)$	Intraband, interband interactions
0 (a)	793.7, 794.0	3.57	796, 796.5	3.12	1.8, 1.4; 0.3
0.5 (b)	795.0, 795.3	3.33	796.6, 797.0	3.07	1.4, 1.3; 0.3
1.0 (c)	795.2, 795.4	2.43	796.5, 796.8	2.34	0.5, 0.5; 0.1
2.0 (d)	796.0, 796.1	2.09	797.0, 797.1	2.04	0.2, 0.2; 0.05
5.0 (e)	796.9, 797.0	2.03	797.7, 797.8	1.97	0.2, 0.15; 0.01
9.0 (f)	796.9, 797.0	2.01	797.5, 797.6	1.95	0.1, 0.1; 0.07

a, is the spectrum collected when focusing near the $3C$-SiC/Si interface. The striking feature in this case is a doublet feature, with a first structure (at about 795 cm^{-1}) and a broader shoulder at slightly higher energy. This doublet structure is nothing but the consequence of the interfacial strain.[6]

Starting from the interface and moving the spot by steps of 0.5 μm toward the SiC surface, we get the two next spectra (labeled b and c) which have been shifted by 250 counts/s for clarity. Two points should be noticed. First, because we collect more and more scattered intensity coming from the SiC layer, the overall intensity increases. Second, the high-energy shoulder which comes from the interfacial strain still reveals at about 0.5 μm from the interface. It disappears around 1 μm. This is nothing but clear evidence of the uniform strain relaxation schematically drawn in Fig. 1(b).

The last three spectra have been collected at about 2, 5, and 9 μm distance from the SiC/Si interface, respectively, and have been shifted by 1, 2.5, and 4.5×10^3 counts/s for clarity. In this case, the interesting results are (i) that, starting 2 μm from the interface, the collected intensity is roughly speaking independent of the spot position and (ii) that, starting about 5 μm from the interface, both the energy position and width of the Raman line do not change anymore. This evidences that a (more or less) constant strain regime has been achieved inside the SiC material.

While the strain regime is more or less uniform, it is not yet homogeneous. This is evidenced by considering the asymmetric line shape, which is better seen for cases $c-f$, where the splitting of the TO doublet is small. The line appears rather sharp on the high-energy side and much smoother on the low-energy one. While the step frequency is constant, there is, for instance, much less experimental points on the right side of the peak (high energy) than there are on the left one (low energy). This asymmetric line shape, which is just the opposite to the one found close to the interface, cannot come from the remaining value of the uniform strain (if any). Obviously, it demonstrates that local strain fluctuations do exist. In other words, we find that, in the region where the uniform strain is more or less constant, there are still large local fluctuations on the scale of the laser spot and that, because of these local fluctuations, the line shape is asymmetric.

Since we have already seen that an asymmetric line with a long low-energy wing indicates a short-range disorder, we have attempted to fit all doublet components with the fluctuation model of Secs. III C 1 and III D. We have found that the anisotropic case (Sec. III D) gives better results. This is because all theoretical curves in Sec. III C 1 drop too sharp on the high-frequency side.

The final comparison of theoretical results with experimental data is shown as solid lines in Fig. 7. The corresponding series of fitting parameters is listed in Table I. The agreement is quite satisfactory, but calls for the following comments.

First, on the different curves, attempting to treat the intrinsic line width $\Gamma^{(\mathrm{int})}$ as an adjustable parameter, we have found that the best fit was always achieved using values in the interval 1.8 ± 0.1 cm^{-1}. This indicates both the quality of sample (and/or the reproducibility of the experiments) as well as the correctness of the theory. As a consequence, the average value $\Gamma^{(\mathrm{int})}=1.8$ cm^{-1} was taken for all lines.

Second, for the doublet lines, there is a rather weak dependence of the complex line shape on the final value of the correlation radius. As a consequence, this quantity has not been adjusted. It was only extracted from the adjustment of

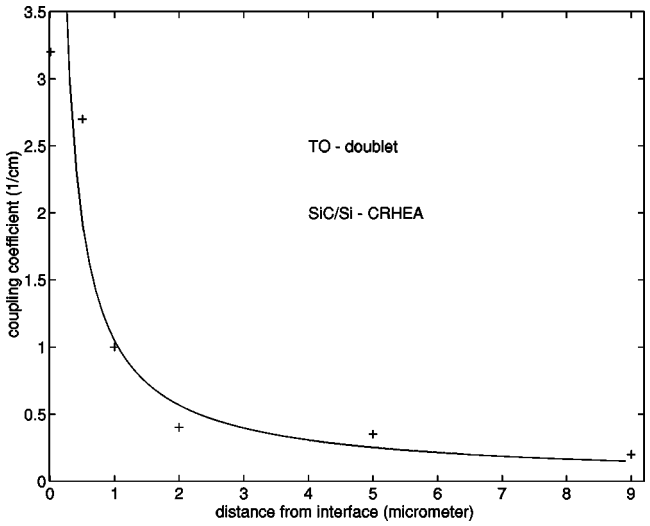

FIG. 8. Strain relaxation (taken from the results of Table I) for the coupling constants $C_{11}+C_{22}$ plotted as a function of the distance from the SiC/Si interface.

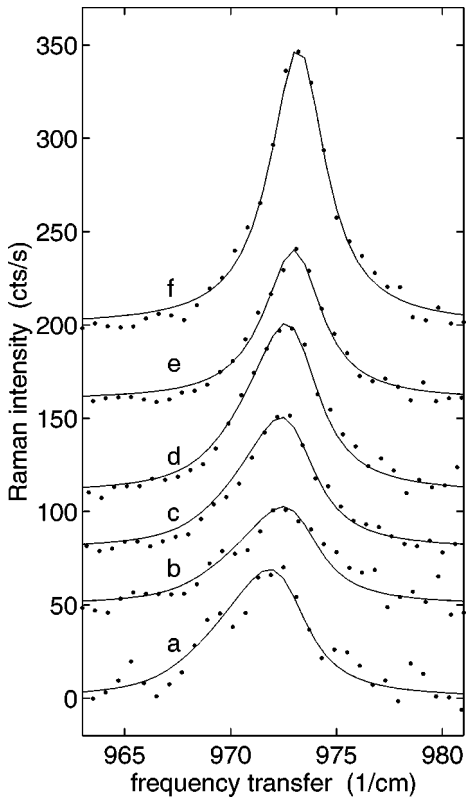

FIG. 9. Same as Fig. 7 but for the LO-phonon singlet. All parameters are listed in Table II.

the longitudinal phonon modes collected in the same run (see Fig. 8) and the same value ($r_0\omega_0/s=20$ which corresponds with about $r_0/a\simeq 6$) was taken in all cases.

The only adjustable parameters appear to be the magnitude of the doublet splitting (which resolves experimentally in Fig. 7, line a, close to the interface) and the interaction constant with the strain fluctuations. Typically, in both cases of (a) the interface spectrum and (b) the spectrum collected 0.5 μm away from the interface, a doublet splitting of the order of 2 cm^{-1} was found. Both the homogeneous strain and the strain fluctuations contribute (for about half of the total value) to this splitting. For additional information, see Table I.

Since the three constants given in the last column, $C_{jm}=\varepsilon^2\omega_0^3 r_0^2 w_{jmmj}/2s^2$ $(j,m=1,2)$, describe the phonon doublet interactions with the strain fluctuations [compare Eqs. (36) and (37) with Eq. (9)], plotting the change in interaction constant (mean square of the homogeneous strain) versus distance to the SiC/Si interface should be proportional to the change in strain magnitude. Such a plot is shown in Fig. 8. Qualitatively speaking, we find a fast relaxation regime which starts right at the interface and extends up to about 3 μm. Then the relaxation (which still continue) become less drastic. We have attempted to fit the data with a $z^{-\alpha}$ dependence (solid line). The final value obtained from a least-mean-square fit procedure gives $\alpha=1.0\pm 0.2$. We emphasize that the two formulas (36) and (37) give the observed values for the width and shift with $w\simeq 1$. Then, if we use $r_0\omega/s=20$ and $C=2$ cm^{-1} as an average value at about 0.25 μm from the interface, we come out with a typical value for the homogeneous strain of $\varepsilon\simeq 10^{-3}$.

TABLE II. Same as Table I but for the LO phonon Raman spectra shown in Fig. 9.

Distance from interface (μm)	LO line $\omega(0),\omega(c)$	Total width $\Gamma(c)$	Intraband interaction coupling
0 (a)	971.3, 971.6	4.02	1.5
0.5 (b)	972.0, 972.4	3.86	1.3
1.0 (c)	972.0, 972.3	3.62	1.0
2.0 (d)	972.3, 972.5	3.45	0.7
5.0 (e)	972.9, 973.0	2.88	0.18
9.0 (f)	973.1, 973.2	2.80	0.1

C. Effect of strain fluctuations on the LO phonon

The effect of strain fluctuations on the LO-phonon Raman spectrum has been already discussed at length in the case of LETI and Cree samples in Ref. 3 and, in this case, both effects of short-range and long-range disorders have been demonstrated. Independent evidence of the short-range disorder effect, which affects the very thick sample from CRHEA, can also be found by inspection of the LO-phonon Raman spectrum in Fig. 9.

Similar to Fig. 7, we display the series of spectra taken from the interface (line a) to about 9 μm away from the interface (line f). Again, they have been shifted for clarity. As already discussed in Sec. III D, the small signal intensity comes because the LO-phonon modes are forbidden in this backscattering configuration. The nice point is that, again, the line shape is asymmetric (with a more pronounced low-energy wing). In this case, fitting all results with the theoretical equations (36) and (37) of Sec. III D, we get the theoretical spectra displayed as solid lines in Fig. 9 and the series of parameters listed in Table II.

Obviously the agreement is very satisfactory and supports the anisotropic short-range disorder picture obtained from the consideration of the TO modes. For the relaxation law we obtain now $\alpha=0.76\pm 0.25$. Within experimental uncertainty, this is in very good agreement with our previous determination.

V. CONCLUSIONS

Investigating, both theoretically and experimentally, the TO- and LO-phonon Raman scattering in strained crystals, we have found that different strain regimes do coexist. First is the average (homogeneous) strain which relaxes smoothly when moving away from the interface. Next are fluctuations, the range of which extends over (typically) the range of optical wavelengths. Both kinds of resulting shift and broadening have been experimentally observed by displacing a laser spot on the lateral side of different 3C-SiC/Si samples and by measuring the Raman cross section as a function of the separation from the heterointerface. Depending on the samples, one can find evidence of either a short-range disorder (this work and Fig. 2 in Ref. 3) or a long-range disorder (see Fig. 4 in Ref. 3).

The theoretical model is based on the solution of Dyson's equation for the averaged phonon Green's function. A first (standard) contribution to the phonon frequency shift [see Eqs. (7) and (8)] comes from the averaged strain that does

exist because of any external stress or interface mismatch. This contribution may be positive or negative, whether the stress is compressive or tensile. For instance, in the case of a SiC/Si interface, it is tensile in SiC and compressive in silicon. While very similar, because of the triple phonon degeneracy, the theoretical analysis of the experiment data in the case of silicon is slightly more complicated. It was not presented in this work but is currently in progress. A second contribution comes from the static strain fluctuations due to dislocations, grain or twin structure, and other structural defects. Because all other phonon states are at lower energy, it is always positive for the top of a phonon singlet [see Eqs. (29), (34), and (37)]. The opposite result would be true for a minimum of the branch. The sum of these two contributions is positive for Si and negative for SiC (and relatively smaller). The phonon broadening results only from the strain fluctuations.

Two limiting regimes have been found, depending on whether the range of strain disorder r_0 is small or large. The crossover (critical) value $r_0 \simeq a\sqrt{\omega_0/\Gamma}/\pi$ is moderately large in the atomic units a. This is of special interest for the problem under consideration since r_0 should be of the order of the strain fluctuation (i.e., the potential radius of the imperfections). This is the existence of a small value for the parameter $\sqrt{\Gamma/\omega_0}$ which provides the physical basis for the present theory.

For the short-range disorder (i), the phonon momentum varies over wide limits in the scattering by strain fluctuations with comparison to the interval determined by the phonon width. If $r_0 \to 0$, the influence of the strain fluctuations on the line width and shift decreases [see Eqs. (27), (29), and (24)]. In the opposite case of a long-range disorder (ii), the phonon is only scattered by the strain fluctuations on a small angle. In this case we can consider very large r_0. The linewidth does not depend on r_0 [see Eq. (32)] but the line shift (34) decreases when r_0 increases. Different line shapes can be observed in the two different regimes. In case (i), the resonance line drops more slowly on the low-frequency side, because the phonon density of states increases below the top of branches. In case (ii), the resonance line is more symmetric but non-Lorentzian.

Because it would appear natural for the disorder to be anisotropic in the presence of an interface, we have also considered the case of a 2D disorder. The correlation radius was taken to be much smaller for the directions parallel to the interface than it was for the direction perpendicular to the interface. We have found that the resulting resonance line does not drop so sharply on the high-frequency side as it does in the corresponding case of a short-range 3D disorder (i). This 2D model gives the best fit to the experimental data for the anisotropic phonon lines. Moreover, we have found that, in this case, the intensity of the disorder (or, more precisely, the mean-squared strain) drops (starting from the interface) according to an approximate z^{-1} dependence. Of course, incomplete strain relaxation occurs in thin samples. This was found in Ref. 3 for a commercial sample with about 3 μm thickness.

Finally, we would like to point out the difference between the present theory and the mechanism of the Fano resonance in any conducting system. The asymmetric line shape in the Fano resonance comes as a result of the electron-phonon interactions. It arises from the imaginary part of the electron loop and does not depend on the phonon density of states.

ACKNOWLEDGMENTS

The authors thank A. Leycuras from CRHEA and C. Jaussaud from LETI-CEA for the gift of samples used in the present work. They also thank H. Capellmann, V. Fateev, G. Güntherodt, A. Iosselevich, and G. Pikus for discussions. One of us (L.A.F.) was supported in the framework of the INTAS program 0101-CT93-0023. He greatly thanks J.L. Robert and A. Neveu for warmly offering hospitality in Montpellier.

*Present address: LMGP-INPG, BP46, 38402 Saint Martin d'Heres, France.

[1] See, for instance, M. A. Capano and R. J. Trew, MRS Bull. **3** (22), 19 (1997) and references therein.

[2] See, for instance, H. Matsunami, in *Amorphous and Crystalline Silicon Carbide II*, Springer Proceedings in Physics Vol. 43 (Springer, New York, 1989), p. 2, and references therein.

[3] L. A. Falkovsky, J. M. Bluet, and J. Camassel, Phys. Rev. B **55**, R14 697 (1997).

[4] F. Cerdeira, C. J. Buchenauer, F. H. Pollak, and M. Cardona, Phys. Rev. B **5**, 580 (1971).

[5] P. Merle, J. Pascual, J. Camassel, and H. Mathieu, Phys. Rev. B **21**, 1617 (1980).

[6] J. M. Bluet, J. Camassel, L. A. Falkovsky, and A. Leycuras, Diamond Relat. Mater. **6**, 1385 (1997); see also J. M. Bluet, L. A. Falkovsky, N. Planes, and J. Camassel, in Proceedings of the International Conference on SiC, III-Nitrides and Related Materials, Stockholm, 1997 [Mater. Sci. Forum **264-268**, 395 (1998)].

[7] P. J. Colwell and M. V. Klein, Phys. Rev. B **6**, 598 (1972).

[8] H. Harima and S.-I. Nakashima, in *Silicon Carbide and Related Materials 1995*, edited by S. Nakashima, H. Matsunami, S. Yoshida, and H. Harima, IOP Conf. Proc. No. 142 (Institute of Physics and Physical Society, London, 1996), p. 365.

[9] B. Friedl, C. Thomsen, and M. Cardona, Phys. Rev. Lett. **65**, 915 (1990).

[10] T. P. Devereaux, A. Virosztek, and A. Zawadowski, Phys. Rev. B **51**, 505 (1995).

[11] L. A. Falkovsky and S. Klama, Physica C **264**, 1 (1996).

[12] L. A. Falkovsky and E. G. Mishchenko, Phys. Rev. B **51**, 7239 (1995).

[13] D. W. Feldman, J. H. Parker, Jr., W. J. Choyke, and L. Patrick, Phys. Rev. **170**, 698 (1968).

[14] Z. C. Feng, W. J. Choyke, and J. A. Powell, J. Appl. Phys. **64**, 6827 (1988).

[15] A. Leycuras, Diamond Relat. Mater. **6**, 1857 (1997).

[16] N. Becourt, J. L. Ponthenier, A. M. Papon, and C. Jaussaud, Physica B **185**, 79 (1993); see also N. Becourt, B. Cros, J. L. Ponthenier, R. Berjoan, A. M. Papon, and C. Jaussaud, Appl. Surf. Sci. **68**, 461 (1993).

[17] C. Dezauzier, N. Becourt, G. Arnaud, S. Contreras, J. L. Ponthenier, J. Camassel, J. L. Robert, J. Pascual, and C. Jaussaud, Sens. Actuators A **46-47**, 71 (1995).

[18] Cree Research Inc., 2810 Meridian Parkway, Durham, NC 27713.